Electron drift velocity in silicon*

C. Canali, C. Jacoboni, F. Nava, G. Ottaviani, and A. Alberigi-Quaranta
Istituto di Fisica dell'Università, Modena, Italy
(Received 16 October 1974)

Experimental results for electrons obtained with the time-of-flight technique are presented for temperatures between 8 and 300°K and fields ranging between 1.5 and 5×10^4 V cm^{-1} oriented along ⟨111⟩, ⟨110⟩, and ⟨100⟩ crystallographic directions. At 8°K the dependence of the transit time upon sample thickness has allowed a measurement of the valley repopulation time when the electric field is ⟨100⟩ oriented. These experimental results have been interpreted with Monte Carlo calculations in the same ranges of temperature and field. The theoretical model includes the many-valley structure of the Si conduction band, acoustic intravalley scattering with correct momentum and energy relaxation and correct equilibrium phonon population, several intervalley scatterings, and ionized impurity scattering.

I. INTRODUCTION

Even though Si is such an important semiconductor, its charge-transport properties have not been fully understood on the basis of microscopic interactions. New circumstances suggest a general reexamination of the problem. The availability of purer material and of the time-of-flight technique[1-5] allows an extension of drift-velocity measurements to lower temperatures, furnishing in this way a complete set of data from almost Ohmic fields up to saturation of the drift velocity in different crystallographic directions, with little effect of impurity scattering. The Monte Carlo[6] technique for solving the Boltzmann equation permits us to abandon those analytical approximations, such as the relaxation time, the diffusion approximation, or an *a priori* choice of the form of the carrier distribution function, which have characterized the previous calculations on high-field transport in semiconductors.[7,8] Furthermore, the Monte Carlo technique allows a correct treatment of intervalley scattering without any assumption of strong or weak coupling between parallel or perpendicular valleys. In this paper the Monte Carlo technique is extended to the case of a zero applied electric field. In this way, the difficulty related to the imprecision of this method in the determination of the drift velocity at low (Ohmic) applied electric fields has been overcome.

The aim of the present paper is to give a wide general picture of electron-transport properties in Si through extensive experimental results and their theoretical interpretation in the light of the particular form of the Si conduction band and the microscopic electronic interactions.

Section II contains a description of the experimental apparatus together with a discussion of the sources of errors in the measurements. Section III contains the experimental results. In Sec. IV we describe the theoretical model and the Monte Carlo programs used for the microscopic interpretation of the electron transport. In Sec. V experimental and theoretical results are compared and discussed.

II. TIME-OF-FLIGHT TECHNIQUE AND EXPERIMENTAL APPARATUS

The time-of-flight technique is based on the measurement of the time that charge carriers created by a suitable ionizing radiation spend to cross, under the influence of an applied electric field, a sample of known thickness W. Since this topic has been recently treated in several papers,[1-5] we will recall here only its principal features. The block diagram of the experimental apparatus is shown in Fig. 1. When the charge carriers are created by an ionizing radiation with a range which is much shorter than W, the carriers of one type are collected after having travelled a negligible fraction of W, while the carriers of the other type, under the influence of a uniform electric field, have to drift across the whole sample with an average velocity v_d and are collected at the opposite electrode after the transit time $T_R = W/v_d$. In this case the shape of the current signal, induced at the ends of the sample is determined only by the motion of the carriers which drift across W. Thus, by a measurement of T_R and W, v_d for one kind of carrier is directly obtained.

The thermalization process of the highly excited carriers produced by the impinging radiation is a complicated mixture of pair production and optical and intervalley phonon emission. In our experimental condition, however, it is much faster than transit across the sample since the measured

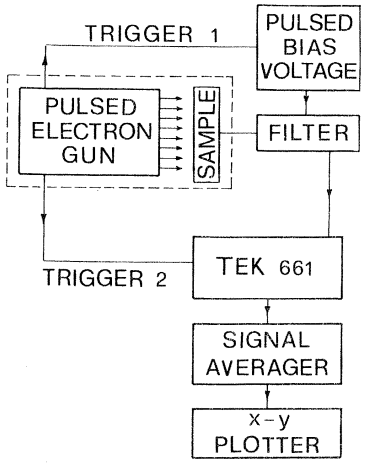

FIG. 1. Block diagram of the experimental apparatus.

drift velocities along a ⟨111⟩ direction are always independent of sample thickness.

Carrier trapping during transit across the sample can modify the waveform and the width of the signal $i(t)$ if T_R is greater than or equal to the mean free drift time τ^+ of the carriers.[4] In our experimental conditions τ^+ is always at least 10^3 times greater than T_R, so that trapping does not appreciably disturb the measurements.

A. Samples

The samples used were surface barrier diodes made of high-resistivity and high-purity n-type silicon supplied by Wacker Chemitronic. Several samples have been obtained from the same ingot cut perpendicular to the crystallographic axes ⟨111⟩, ⟨110⟩, and ⟨100⟩ with an accuracy of about $\pm 1^\circ$. The various samples had a thickness ranging from 200 to 1000 μm and a useful area of about 10 mm^2 approximately placed at the center of 1-cm^2 disks. The sample characteristics are reported in Table I. Hall-effect measurements[9] have given donor and acceptor concentrations around 5×10^{12} cm^{-3}; γ activation analysis[10] has yielded a concentration of O, N, and C, around 7×10^{15} cm^{-3}.

The samples were fitted in between two boron-nitride pierced disks and included in copper containers. The boron-nitride disks guaranteed a good thermal coupling and electric insulation between the samples and the copper container. The devices were mounted on a variable-temperature liquid-helium cryostat (Andonian MDG-7L-30N) and

TABLE I. Characteristics of the samples used in drift-velocity measurements. The material has been supplied by Wacker-Chemitronic.

Sample	Ingot No.	Thickness (μm)	Axis	Resistivity (kΩ cm)	10^3EPD/cm^2	Lifetime (msec)
1	20 591-6	280	[111]	220	15	2
2	20 591-6	450	[111]	220	15	2
3	20 591-6	330	[111]	220	15	2
4	21 593-6	400	[111]	68	0	3.5
5	21 593-6	550	[111]	68	0	3.5
6	21 593-6	600	[111]	68	0	3.5
7	29 246-1	380	[111]	145	21.5	3
8	29 246-1	700	[111]	145	21.5	3
9	29 246-1	650	[111]	145	21.5	3
10	29 246-1	450	[110]	145	21.5	3
11	29 246-1	550	[110]	145	21.5	3
12	34 128-2	330	[110]	30–35	21.5	2
13	21 593-6	250	[110]	68	0	2.5
14	29 246-1	183	[100]	145	21.5	3
15	29 246-1	280	[100]	145	21.5	3
16	29 246-1	450	[100]	145	21.5	3
17	29 246-1	1050	[100]	145	21.5	3
18	21 593-6	330	[100]	68	0	1.8
19	21 593-6	500	[100]	68	0	1.8
20	21 593-6	270	[100]	68	0	1.8
21	39 087-1 II	550	[100]	48	15÷18	···
22	39 087-1 II	650	[100]	48	15÷18	···
23	39 087-1 II	480	[100]	48	15÷18	···
24	55 775-41	430	[111]	3.1	0	1.7
25	58 799-81	250	[111]	0.01	0	···
26	50 503-16	470	[111]	0.1	0	···

could be cooled to 6°K. The sample temperature was measured by means of a calibrated germanium resistance (Scientific Instrument-model 2G), which was mounted in close thermal contact with the sample itself. By means of a dummy sample we have verified that the difference between the temperature of the sample and that of germanium resistance was practically negligible in all conditions. In order to avoid heating and polarization phenomena in the sample, the reverse-bias voltage V_a was applied only for a short time interval (between 20 and 100 μsec) at low repetition rate (between 50 and 150 Hz).

B. Electronic apparatus

Charge carriers were created by sending on the sample bunches of 30-keV electrons, produced by a pulsed electron gun.[11] These bunches generally contained 10^4 electrons each, their duration could be changed from 70 psec to 1 nsec, and their repetition rate was variable at will. Electrons of 30-keV penetrate some 5–10 μm in Si. Variation of the beam current and bunch duration permitted control of the number (10^7–10^9) and density (10^{11}–10^{13} cm^{-3}) of electron-hole pairs produced in the sample.

The current signal $i(t)$ produced by each electron burst was sent to a sampling oscilloscope (Tektronix 661, 4S2A, 5T3) by means of a 50-Ω coaxial cable. The geometry and sample mounting, together with its connection to the coaxial cable were performed in such a way as to make the eddy capacities and inductances as small as possible. The total rise time of the electronic apparatus (including the diode) did not exceed 300 psec. The recording was made by an X-Y plotter (Hewlett Packard 7035 B) connected to the analogic output of the sampling oscilloscope. When the noise-to-signal ratio was too low, a signal-averaging computer (Nuclear Data N.D. 811) was interposed between the analogical output of the sampling and the X-Y plotter. The application of the pulsed bias voltage V_a was adequately anticipated (e.g., 10–20 μsec) with respect to the impact of the ionizing radiation.

C. Experimental sources of errors

A list of errors effecting the drift-velocity measurements as a function of electric field and temperature is reported below with an estimate of their values.

(i) Errors in the measurements of the thickness of the samples. With our apparatus the maximum error is estimated to be less than ±1%.

(ii) Errors in the measurements of the transit time T_R. These errors are different in the low- or in the high-electric-field regions. At low fields, owing to low signal-to-noise ratio, the error is due mainly to the uncertainty in identifying the leading and trailing edges of the current pulse, and the maximum error is around ±3%. At high fields, the transit time T_R is shorter (a few nsec), and the equivalent circuit of the detector modifies the signal shape. However, with a careful selection of the sample thickness, it is possible to reduce the maximum error to ±1%.

(iii) Errors due to a nonuniform distribution of the electric field. In order to use the simple relationship $v_d = W/T_R$ we must assume a constant electric field inside the sample. This assumption is not always totally verified in the surface-barrier diodes used in our experiments. However, its influence on the determination of the drift velocity is very small, reaching values close to 2% only in the worst case.[5] It is possible to reduce such errors by using high-resistivity material and performing the measurements at applied voltages at least two times higher than the depletion voltage. Carrier freezing at low temperatures, by decreasing the value of the depletion voltage, allows measurements in low-resistivity material and reduces the minimum electric field in high-resistivity material. The effect of carrier freezing has been observed both on C-V characteristics and on the current signal waveforms. This latter effect is shown in Fig. 2. Electric-field perturbation due to space charge has been avoided by keeping a low carrier injection level.[12,13]

(iv) Errors in the measurements of applied voltage. The amplitude of the pulsed bias is measured by using a sampling oscilloscope and a digital voltmeter. The maximum error is about ±2%.

Following the previous analysis, the total error in the drift-velocity measurements should be within ±5% at low electric field and ±3% at high electric field. The maximum error in the electric-

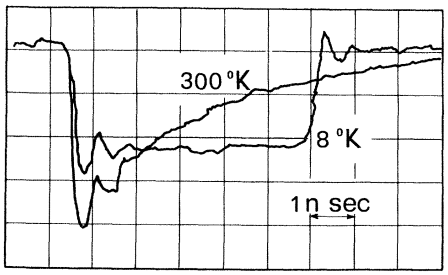

FIG. 2. Current pulses obtained at 8 and 300 °K in a surface-barrier diode made with 3.1 kΩ cm n-type Si. The exponential decay at 300 °K and the square wave shape at 8 °K obtained in the same sample for the same applied voltage indicate that the electric field tends toward a constant and uniform value inside the sample.

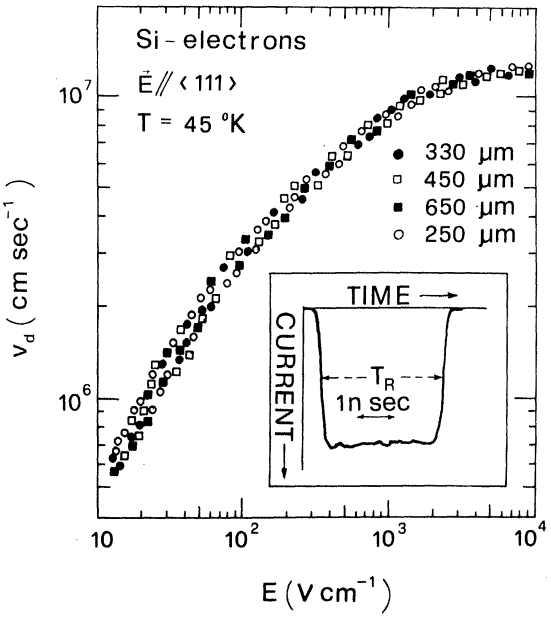

FIG. 3. Typical set of experimental drift velocity v_d obtained at 45 °K in four samples with the electric field E applied parallel to ⟨111⟩ axis. The insert shows the transient current response of the 330-μm sample when 43 V bias voltage is applied. The transit time T_R is 3.4 nsec yielding a drift velocity of 9.7×10^6 cm/sec.

field determination is estimated to be less than ±3%. Finally, the error in the temperature measurements is less than ±1 °K.

We conclude the section of experimental errors by showing a typical set of experimental data. The insert in Fig. 3 shows a current signal obtained at

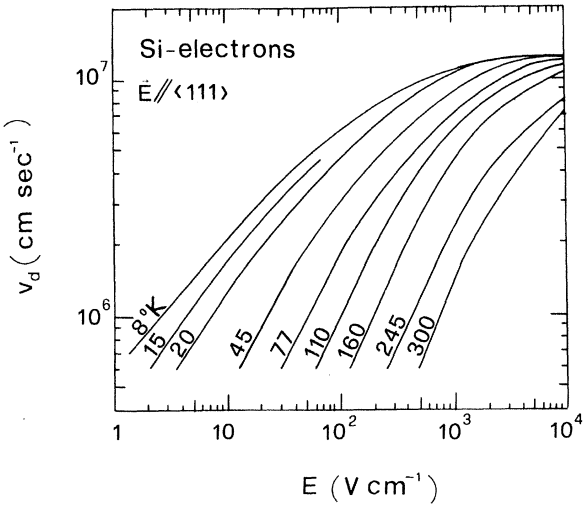

FIG. 4. Experimental electron drift velocity as function of electric field applied parallel to a ⟨111⟩ direction at different temperatures.

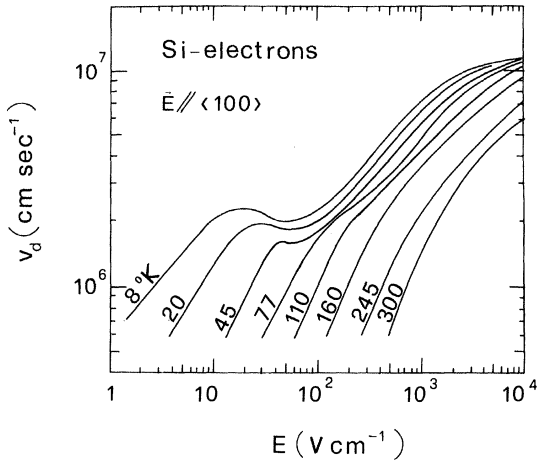

FIG. 5. Experimental electron drift velocity as function of electric field applied parallel to a ⟨100⟩ direction at different temperatures.

45 °K in a sample 330 μm thick with 43 V applied. The transit time T_R measured from the full width half-maximum of the current signal is 3.4 nsec giving a drift velocity of 9.7 10^6 cm/sec. From the shape of the current signal it is possible to deduce that (a) the rise time of the electronic system is less than 300 psec; (b) there is no appreciable evidence of trapping[4] or space-charge effects.[12,13] A series of drift-velocity measurements are shown in Fig. 3 for four samples with the electric field applied parallel to the ⟨111⟩ crystallographic axis. One can easily note that the dispersion of the experimental data obtained with different samples is contained within ±5% in agreement with the maximum evaluated experimental error.

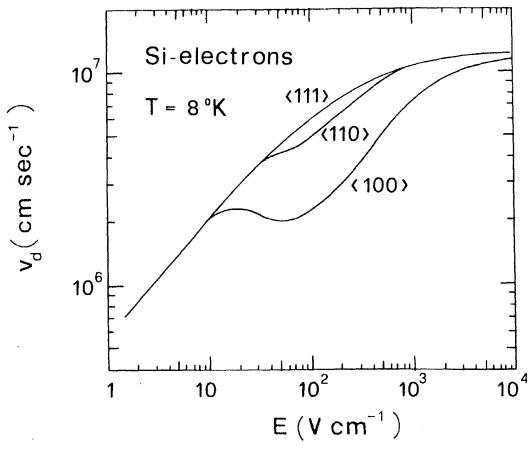

FIG. 6. Experimental electron drift velocity as function of electric field at T = 8 °K with the field applied along the directions ⟨111⟩, ⟨110⟩, and ⟨100⟩; as indicated in the figure.

III. EXPERIMENTAL RESULTS

A. Drift-velocity results

In Figs. 4–6 the electron drift velocity is reported, as a function of temperature and electric field, as solid lines which represent the average value of the experimental data. The electric field ranges from 1.5 to 10^4 V/cm, applied parallel to the ⟨111⟩, ⟨100⟩, and ⟨110⟩ crystallographic axes. The measurements performed with $\vec{E}\,//\langle 110\rangle$ show an appreciable difference with the results obtained with $\vec{E}\,//\langle 111\rangle$ only at 8 °K. Therefore we show the data obtained with $\vec{E}\,//\langle 110\rangle$ only at this temperature (Fig. 6). For the sake of completeness in Figs. 4 and 5, the data in the range (77–300) °K obtained with the same experimental technique and published in a previous paper[5] are partially reported. In order to display the anisotropy effect, the drift velocities obtained at the same temperatures with the electric field applied parallel to the ⟨111⟩ and ⟨100⟩ axes are shown (compared with the theory) in Fig. 7.

The main features of the experimental results are:

(i) The anisotropy effect increases at decreasing temperatures. The curves of the drift velocities along the two directions ⟨111⟩ and ⟨100⟩ tend to join together at a value of the electric field increasing with temperature, even though such a rejoining has not been reached at all considered temperatures.

(ii) At highest electric field applied parallel to a ⟨111⟩ direction a region of drift velocity nearly independent of the electric field is obtained.

(iii) For $T > 45$ °K the Ohmic region is reached and the results are in good agreement with values for the mobility given in the literature.[14–17] For $T \lesssim 45$ °K, even at the lowest applied electric field, the drift velocity is not proportional to the electric field, indicating that Ohmic condition is not reached. At 8 °K a mobility as high as 5×10^5 $cm^2V^{-1}sec^{-1}$ has been obtained at $E = 1.5$ V/cm.

(iv) A negative-differential-mobility (NDM) region was found with $\vec{E}\,//\langle 100\rangle$ for temperatures below 40 °K. The effect is enhanced by decreasing the temperature. The threshold field, defined as the field at which the drift velocity has the maximum value before the region of NDM, decreases

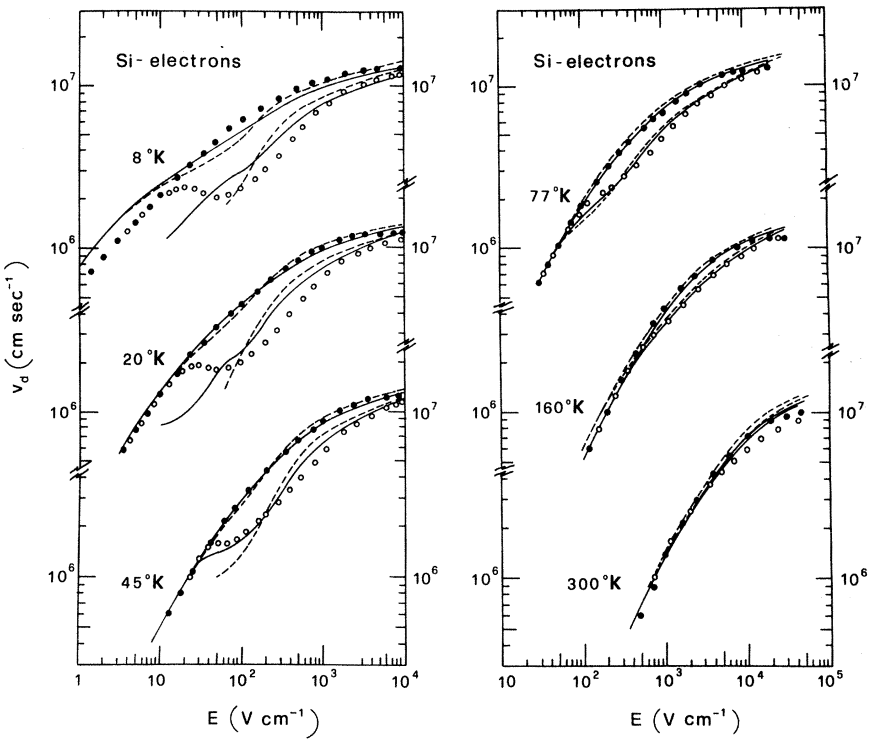

FIG. 7. Electron drift velocity as function of electric field at the different indicated temperatures. Closed and open circles refer to experimental data obtained with the field parallel to ⟨111⟩ and ⟨100⟩ directions, respectively. For the same directions continuous and broken lines indicate the theoretical results obtained, respectively, with sets of parameters A and B, as discussed in the text, and neglecting impurity scattering. Set A contains, and set B excludes, low-energy intervalley phonons. For temperatures ≤ 45 °K the theoretical curves which refer to the ⟨100⟩ direction are interrupted when it was not possible (see text) to reach a sufficient precision in the simulated drift velocity (≤ 3%).

at decreasing temperatures. This effect, however, needs a deeper examination and leads to a new important experimental result, as will be discussed below.

B. Repopulation-time measurements

It is well known that the anisotropy of the drift velocity in silicon is due to a repopulation of the "hot" and "cold" valleys at the minimum of the conduction band.[7] The NDM measured with $\vec{E}//\langle 100\rangle$ is a limiting case of such a repopulation effect.

The electronic transitions necessary to establish this steady-state repopulation are intervalley f transitions (between perpendicular valleys), which require phonons (f phonons) with equivalent temperature T_f of several hundred °K.[18] If the temperature is sufficiently low, the number of such phonons available to perform f transitions with an absorption process is extremely low. Furthermore, at intermediate fields the average electron energy is much smaller than the f-phonon energy $\hbar\omega_f$, and emission processes are also very rare. In such conditions the time necessary to reach steady-state repopulation becomes very long.

It was thus possible to measure, at 8 °K, the repopulation time between hot and cold valleys.[19] Measurements of the transit time T_R with the electric field $\vec{E}$ applied parallel to a $\langle 100\rangle$ direction show, in fact, for E between 10 and 250 V/cm, a strong dependence of the average electron velocity (and NDM effect) upon sample thickness W, this last ranging between 180 and 1050 μm. (The experimental results reported in Figs. 5–7 for 8 °K refer to the longest sample.)

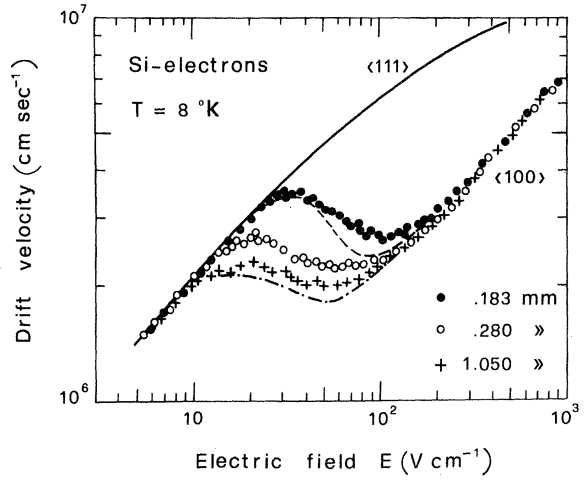

FIG. 8. Electron average velocity as function of applied field parallel to a $\langle 100\rangle$ direction for the different sample thickness indicated in the figure, at $T = 8$ °K. The continuous line indicates for comparison the experimental data obtained, at the same temperature, with the field along a $\langle 111\rangle$ direction. The dot-dashed line indicates the steady-state drift velocity obtained with the procedure discussed in Sec. III B. The dashed line indicates the average velocity of the electrons through a sample with thickness 183 μm evaluated by means of experimental velocities and theoretical repopulation time.

This effect is shown in Fig. 8, where the experimental results obtained for W/T_R in some of the different samples are reported. The continuous line shows the experimental results obtained along a $\langle 111\rangle$ direction. In this figure it may be seen that the experimental W/T_R with $\vec{E}//\langle 100\rangle$ in the shortest samples follow the $\langle 111\rangle$ curve at lower fields and then pass to the $\langle 100\rangle$ curve at higher fields. This is due to the fact that electrons do not have time to reach steady-state conditions, and since anisotropy is essentially due to the valley repopulation, $v_d(\vec{E}//\langle 111\rangle)$ is obtained instead of $v_d(\vec{E}//\langle 100\rangle)$ at lower fields. At higher fields the average electron energy ϵ is higher, the repopulation time is shorter, and steady-state is approached. In longer samples the transit time T_R is longer and steady state is obtained at lower fields.

For a quantitative analysis let $t = 0$ be the time at which the carriers are created at one side of the sample. Since the intervalley transition rates for electrons with $\epsilon > \hbar\omega_f$ are much higher than intravalley rates, while the time necessary to establish the steady-state electronic distribution function f_i within each single valley is much shorter than T_R, we may assume that at $t = 0$ the electrons are equally distributed among the valleys and, within each valley, according to f_i. At $t > 0$ the population $n_c(t)$ and $n_h(t)$ of cold and hot valleys obey the continuity equations

$$\frac{dn_c}{dt} = -n_c P_{ch} + 2n_h P_{hc}\,;$$

$$\frac{dn_h}{dt} = \tfrac{1}{2} n_c P_{ch} - n_h P_{hc}\,, \tag{1}$$

where P_{ch} is the probability per unit time that an electron in a cold valley will jump into a hot valley and inversely for P_{hc}. The solution of Eq. (1) leads to a repopulation exponential with time with a time constant

$$\tau = (P_{ch} + P_{hc})^{-1}\,, \tag{2}$$

and to an average electron velocity

$$v(t) = 2n_c(t)v_c + 4n_h(t)v_h = v_{100} + v_1 e^{-t/\tau}\,, \tag{3}$$

where v_c and v_h are the drift velocity in cold and hot valleys; v_{100} stands for $v_d(\vec{E}//\langle 100\rangle)$; v_1 is a

constant related to P_{ch}, P_{hc}, v_c, and v_h. As we have seen at $t=0$, v is essentially the same as the drift velocity v_{111} obtained at the same field value, and Eq. (3) may be written as

$$v(t) \approx v_{100} + (v_{111} - v_{100}) e^{-t/\tau} . \quad (4)$$

The thickness of the sample is covered in a time T_R such that

$$W = \int_0^{T_R} v(t)\, dt$$

$$= v_{100} T_R + v_1 \tau (1 - e^{-T_R/\tau}) , \quad (5)$$

which for large T_R becomes

$$W = v_{100} T_R + v_1 \tau . \quad (6)$$

This expression can be experimentally tested by directly plotting the sample thickness as a function of the transit time. An example is shown in Fig. 9. The slope of this straight line gives the steady-state drift velocity v_{100} reported in Fig. 8 as a dot-dashed line. v_1 can be obtained as $v_{111} - v_{100}$ and then τ is obtained by the extrapolation of Eq. (6) at $T_R = 0$. The resulting repopulation times are shown as function of field strength in Fig. 10, together with the theoretical interpretation which will be discussed in Sec. V.

C. Complementary measurements

To clarify several experimental aspects of our investigation, complementary measurements have been performed, which deserve to be mentioned at this point.

In order to study the effect of neutral donors on the drift velocity we have performed several measurements at 8 °K, with $\vec{E} // \langle 111 \rangle$ using low-resistivity n-type material with donor concentration (ionized at room temperature) ranging from 10^{13} to 5×10^{15} cm^{-3}. At 8 °K the carriers are frozen and the number of the neutral donors is at least the same as that of conduction electrons at room temperature. No change has been observed in the drift velocity at the lowest applied fields up to neutral donor concentrations of the order of 10^{15} cm^{-3}. This indicates that in our purest samples the effect of the scattering from such centers is negligible with respect to other competing mechanisms.

By changing the energy and/or the number of electrons in the ionizing beam, it was possible to change the concentration of the carriers which travel through the crystal. We have seen no effect on the transit time by changing this density from 10^{11} to 10^{13} cm^{-3}. Such a result seems to indicate that at our concentrations electron-electron scattering is negligible among the processes which determine the drift velocity.

D. Comparison with other experimental data

A comparison of our data with other available data in the literature at temperatures below 77 °K is very difficult, due to the scarcity of published results, particularly for high electric fields.

(i) Current oscillations observed by Asche and Sarbei[20] and Jørgensen *et al.*[21] confirm the existence of an NDM in Si with the electric field parallel to a ⟨100⟩ axis at low temperatures (<40 °K). However, reliable direct measurements of drift velocity in the NDM region had not yet been performed. In fact experimental data of

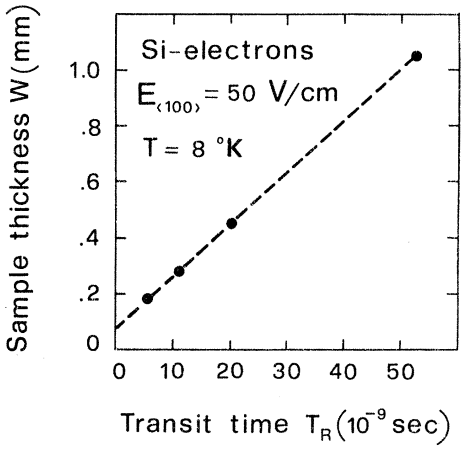

FIG. 9. Sample thickness as function of electron transit time at 8 °K with $E = 50$ V/cm along a ⟨100⟩ direction. The experimental points (dots) are well fitted by a straight line (dashed) as predicted by Eq. (6).

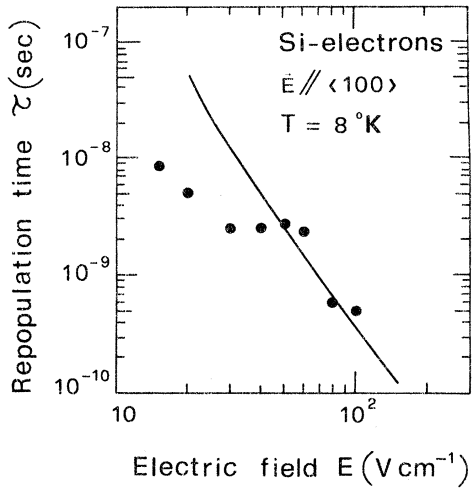

FIG. 10. Repopulation time as function of field strength at 8 °K. Dots indicate the experimental results; the line represents the results of the theoretical Monte Carlo calculation (set A).

Asche and Sarbei[22] show, in the range of field of interest, a region of constant current density, more than a negative differential shape. This behavior is typical of current-vs-voltage measurements performed in negative differential-conductivity region when domains prevail.[22]

The possibility of superseding this fact by using much shorter voltage pulses, as attempted by Jørgensen *et al.*[21] and by Gram,[23] has to confront the difficulty of the necessary repopulation times discussed above. It is worth noting that, at lower temperatures, pulsed-conductivity techniques also find an insurmountable obstacle for their application in the freezing of impurities and the consequent rarefaction of the majority carriers. For this reason the measurements of Asche and Sarbei[20,22] and of Gram[23] do not go below 26 and 34 °K, respectively.

(ii) Saturation drift velocity below 77 °K has been measured by Rodriguez and Nicolet.[24] The comparison of their saturation and our maximum drift velocity as a function of temperature was previously reported and discussed.[5,25]

(iii) Ohmic mobilities have been measured by many authors but a comparison with our data is difficult because (a) for temperatures below 45 °K our experimental data of drift velocity even at the lowest applied electric fields (1.5 V/cm) are not yet perfectly Ohmic; (b) the data in the literature usually do not extend below 20 °K; (c) below 20 °K the data obtained by Norton *et al.*[14] using the photo-Hall technique in order to overcome the freezing of the electrons show a strong effect of impurity scattering.

In Fig. 11 the experimental data of Ohmic mobility obtained by several authors[14-17] with ionized impurity concentration ranging from 3.5×10^{13} to 1.4×10^{14} cm^{-3} are reported as a function of temperature. Our data for the ratio v_d/E, at the minimum applied electric field, also reported in Fig. 11, obtained using material with N_D and N_A of the order of 10^{12} cm^{-3} are in good agreement with the others for temperatures above 45 °K. Below 45 °K our data, even if they are a lower limit of the Ohmic mobility, are the highest ever measured.

In the same figure are also reported the theoretical results obtained with the Monte Carlo method as discussed in Sec. V.

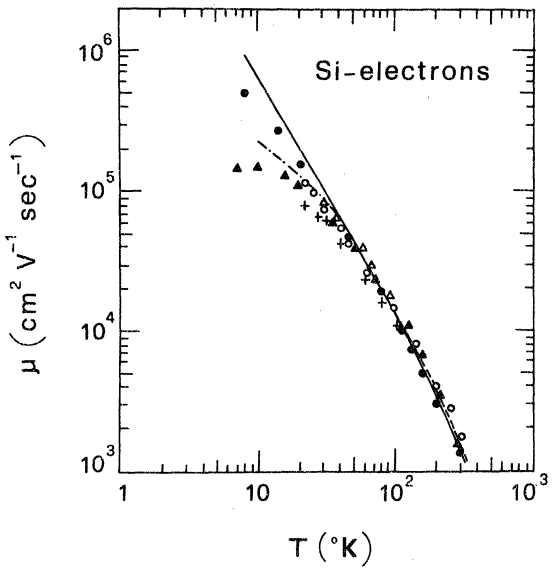

FIG. 11. Ohmic mobility of electrons in silicon as a function of temperature. Closed circles indicate our experimental mobilities at the lowest applied fields, which are perfectly Ohmic only for $T \geq 45$ °K. The other experimental points refer to data from the literature: closed triangles from Ref. 14; crosses from Ref. 15; open triangles from Ref. 16; open circles from Ref. 17. The continuous (broken) line indicates the theoretical results obtained with the set of parameters A (B), neglecting impurity scattering. The dot-dashed line gives the theoretical results with set A and 10^{13} cm^{-3} ionized impurities.

IV. THEORY—MONTE CARLO CALCULATIONS

In Sec. III we presented our extensive collection of experimental results on the drift velocity of electrons in hyperpure silicon over wide ranges of electric field and temperature. In order to interpret these results from a theoretical microscopic point of view, we have used the Monte Carlo method,[6] today generally accepted as the best tool to study transport phenomena, particularly at high fields, when analytical approximations become too unreliable.

Due to the small numbers of travelling electrons in our experimental situation, the phonon populations inside the crystal are assumed to be not disturbed by the presence of the current.

To set up the Monte Carlo program, or, equivalently to write down the Boltzmann equation, we need two fundamental elements of transport theory: the band structure and the electron scattering probabilities.

A. Band structure

The electrons which contribute to charge transport in the conduction band in silicon, even at high applied electric fields, are those in the six equivalent valleys around the six minima of the band along the main crystallographic directions ⟨100⟩. In fact, the other secondary minima, located at the center of the Brillouin zone and along the ⟨111⟩ directions, correspond to very

high energies, of the order of the eV. In the present calculations the ⟨100⟩ valleys have been assumed perfectly parabolic. This is certainly one of the most severe limitations of the present theoretical interpretation.[26] The comparison between experimental and theoretical results will indicate where and in what measure further refinements of the theory are necessary at the present stage.

The energy $\epsilon^{(i)}(\vec{k})$ of an electron in the state $\vec{k}$ in the ith valley is given by[7]

$$\epsilon^{(i)}(\vec{k}) = \frac{\hbar^2}{2}\left(\frac{(\vec{k}-\vec{k}_0^{(i)})_l^2}{m_l} + \frac{(\vec{k}-\vec{k}_0^{(i)})_t^2}{m_t}\right), \tag{7}$$

where $\vec{k}_0^{(i)}$ indicates the position in the Brillouin zone of the center of the ith valley; the subscripts l and t indicate longitudinal and transverse components with respect to the symmetry axis of the valley; m_l and m_t are the longitudinal and transverse effective masses of the electrons; the zero of the energy has been taken at the minimum of the conduction band.

By performing the Herring and Vogt transformation,[27] we write the energy as

$$\epsilon^{(i)} = \hbar^2 k^{2\,*(i)}/2m_0, \tag{8}$$

where $\vec{k}^{*(i)}$ is the transformed of $\vec{k}-\vec{k}_0^{(i)}$ in the ith valley, and m_0 is the free mass of the electrons.

B. Scattering mechanisms

The scattering mechanisms which have been included in the Monte Carlo program are acoustic intravalley scattering, with correct energy relaxation; three f and three g intervalley scattering; intravalley scattering due to ionized impurities.

As regards phonon-assisted transitions, selection rules[28,29] allow acoustic intravalley scattering, f scattering with LA and TO phonons, and g scattering with LO phonons. There are, however, several experimental indications[14,30-34] that other intervalley scattering may be active in electron transport in Si.

Therefore, we have tried to fit our experimental data either including (set of parameter A) or excluding (set of parameter B) the low-energy "forbidden" intervalley phonons. As we shall see, even though the inclusion of these mechanisms is not critical in explaining the Ohmic electron mobility as a function of temperature, it does improve the agreement with experiments when high-field transport is considered.

The contradiction with the selection rules can be due to the fact that these rules are evaluated for electron transitions between points exactly on the ⟨100⟩ axes while, in general, electrons undergo transitions between points relatively far from these axes. For the same reason the energies involved in an intervalley transition is only approximatively given by a single value; a range of energies corresponding to some 10° is certainly involved, and this range increases at increasing temperatures or applied electric fields. Furthermore, it may be noted that for the "forbidden" transitions we expect a k dependence different from that of allowed transitions. However, the theory of intervalley transitions is not sufficiently sophisticated to include this distinction.

As regards impurities, intravalley Coulomb scattering by ionized centers has been included in the present work. The corresponding intervalley transitions are, on the other hand, negligible, due to the large momentum transfer. The intervalley-scattering mechanism considered by Price and Hartmann[35] may be more effective especially in the conditions of long repopulation times. We may note, however, that even intravalley Coulomb scattering by ionized centers has been found to have negligible effect on most of our experimental results, due to the high purity of the samples.

We have also neglected the scattering of electrons by neutral impurities. In fact, the measurements discussed in Sec. III C have shown no effect of neutral donors on the drift velocity obtained in the purest samples.

The effect of neutral impurities such as oxygen has been studied by Logan and Peters[17]; from their results we may conclude that in our samples these impurities may give a small contribution to the transport phenomenon only at the lowest considered temperatures.

Electron-electron scattering is by far the most difficult mechanism to treat in transport theory, since it makes the Boltzmann equation nonlinear in f. The influence of this mechanism has been recently studied, and very little effect on the drift velocity has been found.[36,37] It seems reasonable to expect that its major effect in silicon will consist of reducing the anisotropy due to valley repopulation,[38] by reducing the difference of the average electron energies in the different valleys. Asche *et al.*[38] and Nash and Holm-Kennedy[39] have, in fact, observed this effect experimentally for carrier concentrations above 10^{15} or 10^{14} cm^{-3}. We have seen, on the other hand, that our concentrations are at least one order of magnitude lower, and that the measured times of flight are independent of the injection level in our range. We have therefore neglected, in the present calculations, the possibility of electron-electron scattering. We describe in the Appendix how the

scattering mechanisms have been introduced in the calculations.

C. Monte Carlo program

Our Monte Carlo program is essentially of the type described by Fawcett and Paige[40] for germanium. All six valleys, however, have been included explicitly in the program, checking *a posteriori* in the results the equivalence of the valleys equally oriented with respect to the applied electric field. Rees self-scattering has been used in such a way as to give a step-shaped total scattering rate.[41] The statistical uncertainty of the results has been obtained as standard deviation of many independent calculations and the simulations have been carried on until this uncertainty was less than few percent in the drift velocity, where not otherwise explicitly stated.

It is well known that Monte Carlo calculations become less accurate as the field is lowered. In fact, the drift velocity is obtained as the average velocity of the "sampling" electron; when the electric field E is so low that this velocity is only a small fraction of the thermal velocity, the relative statistical uncertainty on this average value becomes very large, and tends to infinity, for a fixed simulation time, when E tends to zero. Therefore, this difficulty may become crucial in the determination of the Ohmic mobility.

A second difficulty arises from the many-valley model used in the Monte Carlo procedure. At low temperatures when the electric field is not high enough to warm up the electrons to the energy of intervalley phonons, intervalley scattering is much less frequent than intravalley (cf. Sec. III B) and the time average of a single sampling electron does not give a good average over the different valleys. In particular, the valley populations may be affected by large statistical errors,[42] even though the distribution functions of single valleys may be accurate.

1. Monte Carlo for Ohmic transport

To avoid the first difficulty, of the accuracy at Ohmic fields, we have devised a special Monte Carlo program for the determination of the Ohmic mobility μ at $E=0$, based on a determination of the diffusion coefficient[43,44] D and the use of Einstein relation

$$\frac{d}{dt}\langle z^2(t)\rangle = 2D = \frac{2\mu KT}{e}, \tag{9}$$

where $z(t)$ is the distance covered by the simulated particle along a direction z during a time t.

The program is a normal Monte Carlo program with $E=0$. The path of the particle is split into many parts of equal time duration Δt (several Δt's must be considered). The average square distance $\langle z^2(\Delta t)\rangle$ covered during this time Δt is then plotted as function of Δt. For sufficiently high statistics the linearity predicted by Eq. (9) is obtained, and the slope of this straight line yields the value of the mobility. It is important to note that by setting $E=0$, the energy of the sampling carrier is constant during each single flight and there is no need to introduce Rees self-scattering.

In order to cover the temperature range in which, in our simulative runs, intervalley f scattering is absent, we have simulated the history of six electrons at the same time, with initial $\vec{k}$ situated in the six valleys.

The determination of the drift velocity with the standard Monte Carlo method ($\vec{E}\neq 0$ parallel to a $\langle 111\rangle$ direction) has been performed down to values of the electric field as to recover the results obtained with the Ohmic Monte Carlo.

2. Valley average and repopulation

Let us now turn to the second problem: At sufficiently low fields and temperatures, as we have seen, intervalley transitions are very rare, and the simulation does not give an accurate steady-state value of the population of the valleys. The resulting drift velocities are then correct only if the field is applied along a crystallographic direction ($\langle 111\rangle$ in silicon) which "sees" the valleys as equivalent, that is all equally oriented with respect to the field. If, on the contrary, $\vec{E}$ is applied along a different direction, like, for example, a $\langle 100\rangle$ direction in silicon, then very long simulation times may be necessary to obtain this steady-state repopulation.

The situation may be improved by using the distribution function, as obtained in each valley with the Monte Carlo calculation, and the f-transition probabilities, to evaluate the valley repopulation.[42] Steady-state conditions require, in fact, that the number of electrons passing in the unit time from hot-to-cold valleys be equal to the number of electrons which perform the opposite transition. If the field is applied along a $\langle 100\rangle$ direction we have two cold valleys and four hot valleys, and the above condition gives

$$2n_c \int f_c P_f(\epsilon)\, d\epsilon = 4n_h \int f_h \tfrac{1}{2} P_f(\epsilon)\, d\epsilon, \tag{10}$$

where n_c and n_h are the fractions of the electrons in a cold and a hot valley, respectively ($2n_c + 4n_h = 1$); f_c and f_h are the energy distribution functions, normalized to 1, in cold and hot

TABLE II. Set of physical parameters used in the present calculations. Set A and B refer to two different models used to fit experimental results.

Name	Symbol	Set A	Set B	Units	Ref.
First intervalley f scattering f_1					
Equiv. temp.	T_{f1}	210	...	°K	45
Coupl. const.	D_{f1}	1.5×10^{7}	...	eV cm^{-1}	...
Second intervalley f scattering f_2					
Equiv. temp.	T_{f2}	500	500	°K	45
Coupl. const.	D_{f2}	3.4×10^{8}	3.0×10^{8}	eV cm^{-1}	...
Third intervalley f scattering f_3					
Equiv. temp.	T_{f3}	630	650	°K	45
Coupl. const.	D_{f3}	4×10^{8}	4×10^{8}	eV cm^{-1}	...
First intervalley g scattering g_1					
Equiv. temp.	T_{g1}	140	...	°K	45
Coupl. const.	D_{g1}	5×10^{7}	...	eV cm^{-1}	...
Second intervalley g scattering g_2					
Equiv. temp.	T_{g2}	210	...	°K	45
Coupl. const.	D_{g2}	8×10^{7}	...	eV cm^{-1}	...
Third intervalley g scattering g_3					
Equiv. temp.	T_{g3}	700	700	°K	45
Coupl. const.	D_{g3}	3×10^{8}	8×10^{8}	eV cm^{-1}	...
Acoustic deformation potential	E_1	9.0		eV	...
Longitudinal effective-mass ratio	m_l/m_0	0.9163		...	46
Transverse effective-mass ratio	m_t/m_0	0.1905		...	46
Sound velocity	v_s	9.037×10^{5}		cm sec^{-1}	47
Density	ρ	2.329		g cm^{-3}	48
Dielectric const.	κ	11.7		...	49

valleys; P_f is the total f transition rate. By separating the energy axis into discrete equal intervals, the repopulation ratio α is obtained from Eq. (10) as

$$\alpha \equiv \frac{n_c}{n_h} = \sum_i f_h^{(i)} P_f^{(i)} \Big/ \sum_i f_c^{(i)} P_f^{(i)}, \tag{11}$$

where $f_h^{(i)}$ and $f_c^{(i)}$ are the fractions of time spent by an electron in the ith energy interval, in hot and cold valleys, respectively; $P_f^{(i)}$ is the average f-transition rate for an electron in the ith interval.

The average drift velocity is then easily obtained as

$$v_d = [1/(\alpha+2)](\alpha v_c + 2v_h), \tag{12}$$

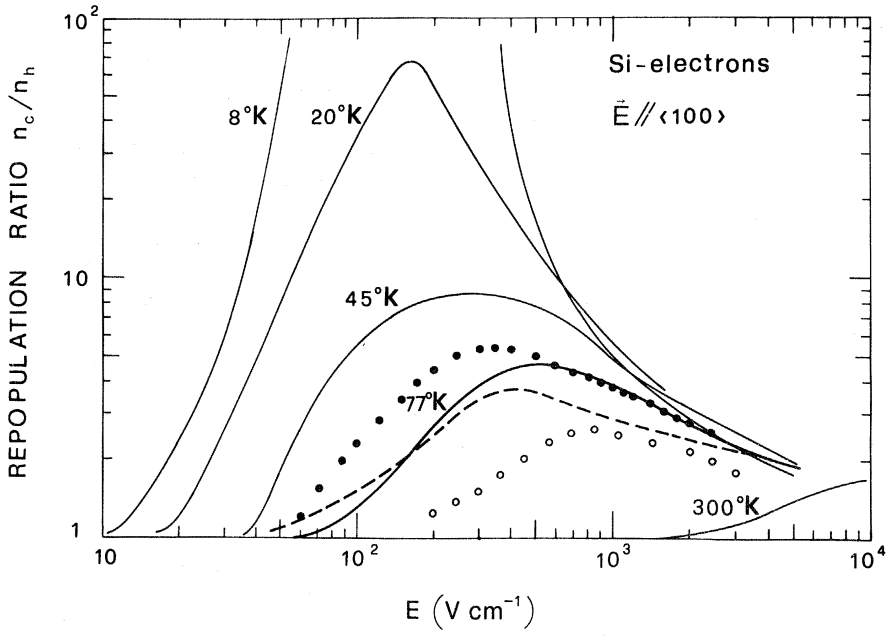

FIG. 12. Repopulation ratio of cold-to-hot valley as function of field applied along a ⟨100⟩ direction at various temperatures (continuous lines) as obtained with the scaling technique. Closed and open circles indicate the results at 77°K in Refs. 39 and 51, respectively. The dashed line indicates the results of the theoretical Monte Carlo calculation (set A) at 77°K.

where v_c and v_h are the partial drift velocities of electrons in cold and hot valleys, obtained by the Monte Carlo simulation.

However, in order to get correct results for the valley repopulation ratio with the above technique, the tails of the distribution functions in hot and cold valleys must be known with sufficient accuracy for energies above the energy of f intervalley phonons. This again requires prohibitive simulation times in certain ranges of electric field and temperature, even though these ranges are diminished with respect to the case of the direct determination of the average electron velocity. For this reason at low temperatures with $\vec{E}$//⟨100⟩ some of the theoretical curves discussed in Sec. IV C 3 are interrupted.

The long simulation times we have just discussed correspond to actual long physical times necessary to reach stationary conditions. The effect has been observed experimentally, as discussed in Sec. III B. The Monte Carlo procedure is, again, a powerful mean to study this transient transport phenomenon. In our case, for example, the simulation first indicated the effect, which was then observed experimentally.

3. *Physical parameters*

In Table II the physical parameters used in the calculations are indicated.[50] As discussed above, sets A and B of the electron-phonon coupling constants correspond to two different attempts to fit the experimental data with (set A) or without (set B) the low-energy intervalley phonons "forbidden" by selection rules.

The value for the acoustic-phonon coupling constants is determined by the Ohmic mobility at 45°K, where the $T^{-3/2}$ experimental slope of $\mu(T)$ ensures that acoustic scattering is dominant. The over-all weight of intervalley coupling constants is determined by the Ohmic mobility at higher temperatures and by the high-field curves with $\vec{E}$ // ⟨111⟩, while the relative importance of f and g scattering is determined essentially by the anisotropy effect as function of temperature and electric field. For the least energetic f transition the coupling constant has been determined by the fitting of the valley repopulation time at 8°K.

The remaining parameters are known in the literature and are derived from measurements independent from transport phenomena.

A discussion of the results is given in Sec. V.

V. DISCUSSION OF RESULTS

In Figs. 7, 8, and 10–13 a comparison is given between experimental and theoretical results.

A. Ohmic mobility

Figure 11 shows the Ohmic-mobility data as a function of temperature of various authors[12–15] together with our experimental values of v_d/E obtained at the lowest applied fields. The continuous and dashed lines represent the results of the present theoretical calculations with the set of parameters (A) which includes low-energy intervalley phonons or, respectively with the set

(B), which does not consider such mechanisms.

For temperatures higher than 30°K the agreement between theory and experimental data is good both in case (A) and (B), indicating that scattering by low-energy intervalley phonons, forbidden by selection rules, would not be necessary if it were only for the temperature dependence of Ohmic mobility.[51] At lower temperatures the experimental data of the other authors tend to be independent of temperature as effect of neutral and ionized impurity scattering. The dash-dotted line represents the result of the present theory (set A or B indifferently) with an ionized impurity concentration $N_I = 10^{13}$ cm^{-3}. This curve lies above the Ohmic data obtained by Norton *et al.*,[14] and the disagreement increases at decreasing temperatures. In the analysis of their data, Norton *et al.* consider, in fact, a similar concentration of ionized impurities accompanied by a contribution of neutral impurities which dominates at the lowest temperatures.

Our experimental data for v_d/E at low temperatures are higher than those reported in literature, which indicates a higher purity of our samples. The same data, however, are lower than the pure-lattice theoretical Ohmic mobility; as we shall see, this effect is due both to heating of the carriers and to impurity scattering.

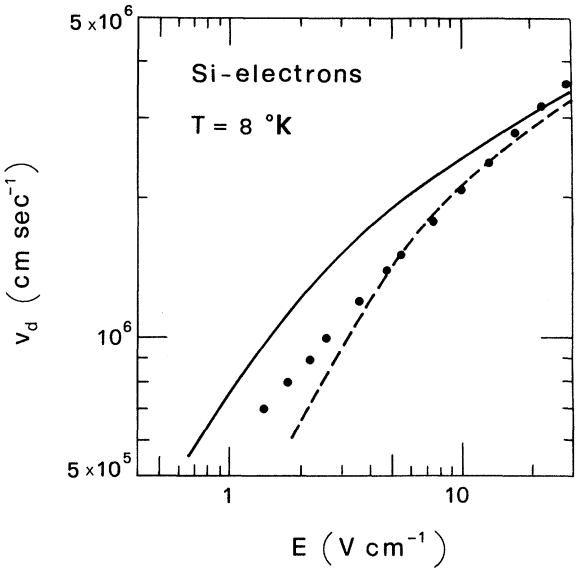

FIG. 13. Electron drift velocity as function of electric field applied parallel to a ⟨111⟩ direction, at 8°K. Circles refer to experimental data. The lines refer to theoretical results obtained with set of parameters A without (continuous line) and with (dashed line) the contribution of 4×10^{12} cm^{-3} ionized impurities.

B. Drift velocity versus field

Figure 7 shows experimental and theoretical drift velocities as functions of temperature and electric field. Drift velocities obtained in both ⟨111⟩ and ⟨100⟩ directions of the applied field are shown together at a given temperature. Closed and open circles represent the experimental data. The continuous and dashed lines give the theoretical results obtained in absence of impurity scattering, with the set of parameters A and B, respectively.

At temperatures ≤ 45°K the theoretical lines for the ⟨100⟩ direction are interrupted in the region of electric fields where too long simulation times are necessary to get a sufficient precision (at least 3%) of the results.

It can be seen that the agreement between experimental and theoretical results is improved if low-energy intervalley phonons (set A) are included. Without such scattering mechanisms (set B) at $T < 45$°K the transport process is controlled by acoustic scattering up to higher electron heating, which is to say up to higher field strengths. Thus at intermediate fields the absence of low-energy intervalley phonons gives a higher electron heating which in turn results in a lower drift velocity. Furthermore, due to the rapid increase in electron energy a too large anisotropy is obtained at intermediate fields and too small at high fields.

At the lowest temperatures a discrepancy can be seen between experimental and theoretical anisotropy (even with set A) at lower fields. This should be due to a mechanism, such as electron-electron scattering or intervalley impurity scattering, which represses the valley repopulation at these fields, and which is not included in the theory.

A structure in the theoretical curves for $\vec{E} \,/\!/\langle 100\rangle$ can be seen at the lower temperatures. It is due to the successive onset of the different f scatterings at increasing mean electron energy. This effect is related to the use of single values for the intervalley phonon energies. As we discussed above, a range of energies is actually involved for each mode of transition. It is not surprising, therefore, that the structure is not seen in the experimental data.

The better agreement with the experimental data obtained with inclusion of low-energy intervalley phonons points toward the conclusion that such scattering mechanisms do contribute to electron transport in silicon, in agreement with the other experimental evidence quoted above (Sec. IV).

At the higher temperatures, disagreement be-

tween the theoretical curves and the experimental results can be seen, at the highest values of the applied field, at which the theoretical values are too high. It was not possible to obtain a better agreement by increasing the coupling strength of some electron-phonon interaction without lowering the theoretical Ohmic mobility around 300°K below the experimental value. Due to the high mean electron energy reached at such high fields it is reasonable to assume that other effects will occur, which are not included in the present model. In particular, nonparabolicity of the conduction band will certainly cause a lowering of the drift velocity at the highest fields.[26]

C. Valley repopulation

From the experimental results of the drift velocity as function of electric field oriented along ⟨111⟩ and ⟨100⟩ directions, it is possible to obtain an approximate value for the valley repopulation ratio using the scaling technique introduced by Schweitzer and Seeger[52] for Ge and applied to Si by Holm-Kennedy and Champlin.[53] The repopulation ratio resulting from the present drift velocity results are shown in Fig. 12 as function of field strength ($\vec{E}//\langle 100\rangle$) at various temperatures. For $T = 77$°K the present results are compared with results of Nash and Holm-Kennedy[39] obtained with the same procedure, and of Vorobyov *et al.*[54] obtained with refractive-index anisotropy measurements. Comparison is also made in Fig. 12 with the results obtained with the Monte Carlo theoretical calculations (set A).

The scaling technique used to determine the repopulation ratio has been tested within the Monte Carlo calculation and found to be accurate within about 10%.

D. Repopulation time

Theoretical values of the repopulation time τ can be obtained from Eq. (2) where P_{ch} and P_{hc} are obtained from the simulated distribution function. In Fig. 10 the results for 8°K are compared, as a function of field strength, with the experimental data obtained as indicated in Sec. IIIB. In fitting the results for τ we have given more importance to its lower values since when τ becomes very long other mechanisms (as, e.g., intervalley impurities scattering) may contribute to lower its value. The dashed line in Fig. 8 indicates the average velocity of the electrons through a sample with thickness 0.183 mm evaluated by means of Eq. (5) (solved numerically for T_R) where $v_1 \approx v_{111} - v_{100}$ is taken from experiments and τ from the theoretical results. A previous account of this effect has been given in Ref. 19, where a less-refined theoretical model was used.

E. Ionized impurity effect

In Fig. 7 it may be seen that at 8°K the theoretical values of the drift velocity v_{111} obtained at the lowest fields without impurity scattering are higher than the experimental data. Such an effect can be ascribed to the presence of ionized impurities. Figure 13 shows for $\vec{E}//\langle 111\rangle$ the experimental data and the theoretical curves obtained with the parameters of set A with and without the inclusion of ionized impurity scattering. An impurity concentration of the order of 10^{12} cm^{-3} improves the agreement between theory and experiments.

At the lowest applied fields the experimental

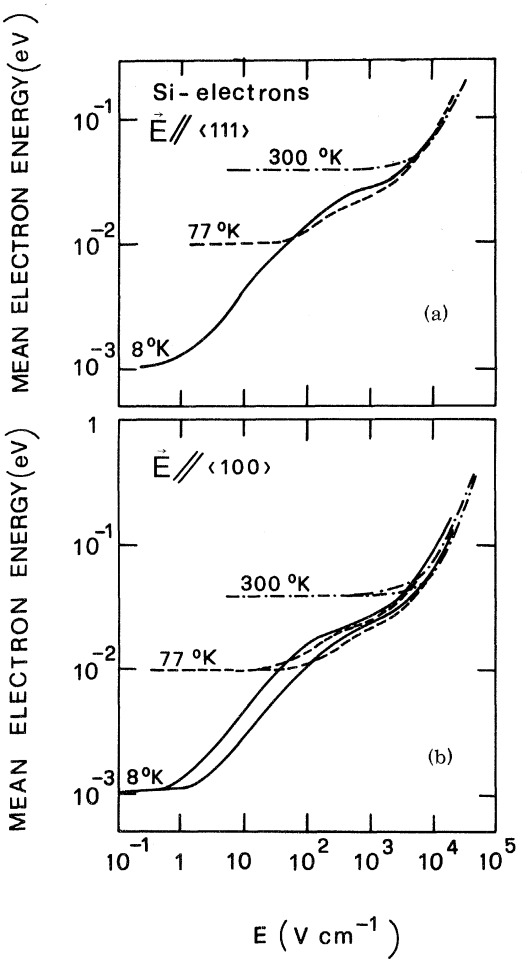

FIG. 14. Mean electron energy as function of electric field at the different indicated temperatures, obtained with Monte Carlo calculations (set A, no impurities). (a) Results obtained with $\vec{E}//\langle 111\rangle$; (b) mean electron energies obtained for hot and cold valleys with $\vec{E}//\langle 100\rangle$.

drift velocity is not yet proportional to the field strength. The theoretical calculations, too, indicate that at such fields the electrons are slightly heated up over the equilibrium thermal energy. We may therefore conclude that at the lowest temperatures our experimental mobilities shown in Fig. 11 are lower than the pure-lattice theoretical Ohmic mobility because of both heating of the carriers and ionized impurity scattering.

F. Electron mean energy

From the same theoretical model used to fit the experimental drift velocity we can obtain all other information necessary to have a full picture of the transport phenomenon such as, in particular, the electron mean energy, the distribution function, and the relative importance of the various scattering mechanisms. In what follows we shall report some of the results obtained for these quantities only with set of parameters A.

Figure 14 shows the electron mean energy as a function of the applied field for different temperatures and field orientations. In Fig. 14(a) the mean energy of all electrons is shown for the electric field applied along a ⟨111⟩ direction, while the mean energies of electrons in cold and hot valleys are shown for $\vec{E}\,/\!/\langle 100\rangle$ in Fig. 14(b).

It may be seen in this figure that at lattice temperature $T = 8°\mathrm{K}$ the average electron energy, independently of field orientation, first increases very rapidly, as long as acoustic modes control the energy balance. At higher fields, when the average electron energy is comparable with the energy of the intervalley phonons, these scattering mechanisms dominate more efficiently the dissipation of electron energy which then increases at a minor rate. At very high fields, the increase of electron energy is again very fast toward electrical breakdown. For $T \gtrsim 77°\mathrm{K}$ intervalley phonons are already effective even at Ohmic fields and the first rapid growth of electron energy is missing.

Another interesting feature of Fig. 14 is that, for $T \lesssim 77°\mathrm{K}$ the electron mean energy at high fields tends to be independent of the lattice temperature. This is due to the high electron average energy at which the emission processes (independent of T, since stimulated emission is negligible) dominate over absorption. This limit, at which the phonon population in the crystal can be assumed zero, is known as zero-point limit. Such a limit is reflected in the low dependence of the drift velocity on temperature at high fields and low temperatures. At $T > 77°\mathrm{K}$ the population of intervalley is not negligible and the zero-point limit is not reached. As a consequence, both electron mean energy and drift velocity are temperature dependent even at the highest applied field strengths. The temperature dependence of the maximum drift velocity obtained experimentally confirms the above discussion in all the temperature range considered here.

G. Energy and velocity dissipation rates

The above discussion on the control of the mean electron energy by the various scattering mechanisms is clarified in Fig. 15. In this figure the energy [Fig. 15(a)] and velocity [Fig. 15(b)] dissipation rates for all considered scattering mechanisms are shown (with the set of parameters A) as a function of the applied field $\vec{E}\,/\!/\langle 111\rangle$ at the intermediate temperature $T = 45\ °\mathrm{K}$. It may be seen here that the dissipation of energy due to acoustic phonons is far from being negligible. At

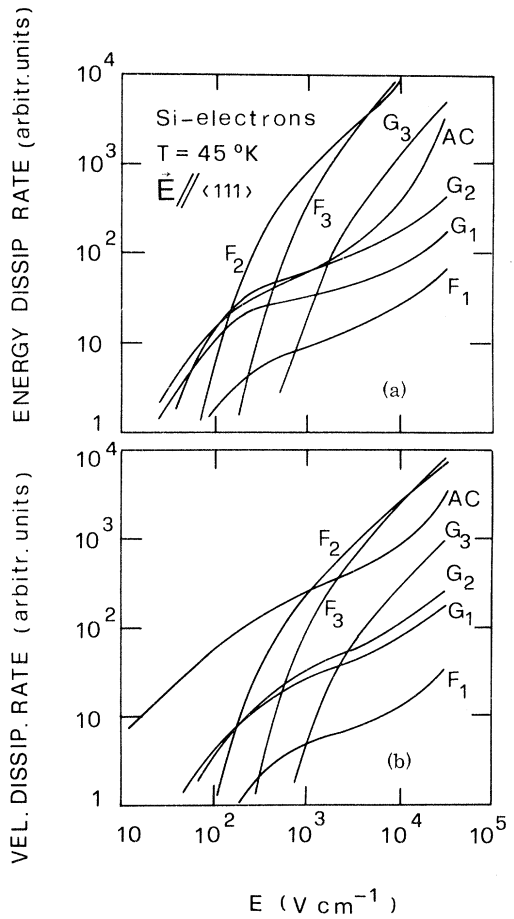

FIG. 15. Monte Carlo results (set A, no impurities) for the energy (a) and velocity (b) dissipation rates due to the various scattering mechanisms as function of field applied along a ⟨111⟩ direction at 45 °K. The symbols refer to the scattering mechanisms as in Table II.

this temperature they constitute the most effective dissipation mechanism up to $E = 100$ V/cm. Their relative importance, as said above, decreases at increasing lattice temperature and electric field.

A general feature of Fig. 15 is that low-energy intervalley phonons become effective at lower fields with respect to high-energy intervalley phonons and then their effect increases less rapidly with field strength due to their smaller coupling with the electrons.

H. Electron-distribution function

Finally, in Fig. 16 the electron-distribution function is shown as a function of energy at 77 °K for an electric field $E = 400$ V/cm. The continuous line refers to all electrons when $\vec{E}$ is parallel to $\langle 111 \rangle$ direction. The dashed and dot-dashed lines refer to $\vec{E} // \langle 100 \rangle$ for electrons in all cold and all hot valleys, respectively. These curves have been normalized to the same total number of electrons, that is, the integral of the continuous line is equal to the sum of the integrals of the other two curves. The energies of the intervalley phonons included in the theoretical model (set A) are indicated in the figure by arrows whose lengths are proportional to the corresponding coupling constants. Due to the large numbers of these phonons the distribution functions exhibit a continuous variation of slope which cannot be described even by a many-temperature Maxwellian. This fact emphasizes again that exact numerical techniques should be used to solve the Boltzmann equation, rather than postulating simple analytical approximations for the distribution function.

VI. CONCLUSIONS

In this paper we have presented an extensive investigation, both experimental and theoretical, of electron-transport properties in Si. In particular, the drift velocity of electrons has been measured with the time-of-flight technique in wide ranges of temperatures and electric fields. The technique, especially suitable for high-resistivity material, allowed us to perform the measurements on high-purity samples, on which an electron mobility as high as 5×10^5 cm^2 V^{-1} sec^{-1} has been obtained at 8 °K, very close to the theoretical pure-lattice mobility. At the same temperature it has also been possible to measure the repopulation time of cold valleys for $\vec{E} // \langle 100 \rangle$.

The theoretical interpretation of the experimental results has been performed with the Monte Carlo technique, taking into account the many-valley structure of Si conduction band and the ellipsoidal shape of the equienergetic surfaces. Particular care has been devoted to the energy balance due to acoustic intravalley modes at low temperatures.

The comparison between theory and experimental data has shown that while low-energy intervalley phonons, forbidden by a restrictive application of selection rules, are not crucial to explain the Ohmic mobility as a function of temperature, their inclusion in the present model is necessary to fit the drift-velocity data as function of temperature, field strength, and field orientation, as well as the valley repopulation time at 8 °K.

Besides the interpretation of the experimental data, from the theory it has been possible to

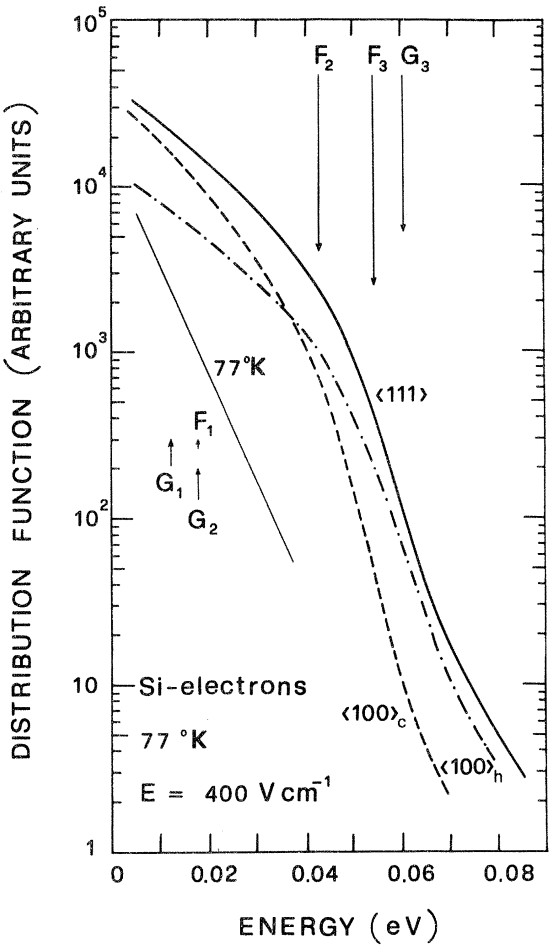

FIG. 16. Energy-distribution function of electrons as obtained at 77 °K with Monte Carlo calculations (set A, no impurities) with an electric field $E = 400$ V cm^{-1}. The continuous line refers to all electrons for $\vec{E} // \langle 111 \rangle$; the dashed and dot-dashed lines refer to $\vec{E} // \langle 100 \rangle$ for electrons in all cold and all hot valleys, respectively. The slope of the straight line corresponds to the lattice temperature. The arrows indicate the energies of intervalley phonons, and their lengths are proportional to the corresponding coupling constant.

obtain those particular sets of information, such as the mean electron energy, the dissipation rates of energy and velocity by the various scattering mechanisms, the electron distribution function, and the valley repopulations, all of which contribute to obtaining a complete physical picture of electron transport in silicon.

ACKNOWLEDGMENTS

The authors wish to thank Dr. L. Reggiani and Dr. M. Costato for helpful discussions. P. Cantoni and M. Bosi are acknowledged for the help in collecting the experimental data.

APPENDIX

We shall here describe how the different scattering mechanisms have been included in our Monte Carlo calculations.

Intravalley acoustic scattering

Acoustic-phonon scattering must be treated with special care in a Monte Carlo calculation of electron transport at low temperatures. In fact the energy exchange between electrons and lattice due to this mechanism is very small even with respect to the electron energy,[7] but the small amount of energy exchanged in these collisions ensures stationarity when a small electric field is applied, since in these conditions no other dissipative mechanisms are appreciably effective. If the scattering is approximated with an elastic process, when a dc electric field is applied, no matter how small its strength, the electrons are artificially warmed up at an energy of the order of magnitude of that of the less energetic intervalley phonon. A wrong balance of electron energy may result also if the phonon population or the energy exchanged in each single collision are not taken into account with sufficient precision.

On the contrary, the angular dependence of the matrix elements can be averaged into a matrix element which does not depend on the direction of the phonon wave vector $\vec{q}$ involved in the transition, without introducing inconsistencies in the calculations. We have made this approximation in the present calculation. It may effect the results of a few percent only in the region of warm electrons at low lattice temperatures (below 77 °K). At higher temperatures or higher applied fields electrons have enough energy to perform intervalley transitions, and the influence of acoustic phonons diminishes, while at Ohmic fields due to the cubic symmetry of the crystal the mobility reduces to a scalar quantity and the angular dependence of the scattering is summed up in the (unknown) coupling constant.

TABLE III. Limits of integration of the variable $x = \hbar q v_s/KT$ for acoustic scattering.

$\epsilon \le \epsilon_s^*$	Absorption	$x_1 = \frac{4\epsilon_s^{*1/2}}{KT}(\epsilon_s^{*1/2} - \epsilon^{1/2})$
		$x_2 = \frac{4\epsilon_s^{*1/2}}{KT}(\epsilon_s^{*1/2} + \epsilon^{1/2})$
	No emission	
$\epsilon > \epsilon_s^*$	Absorption	$x_1 = 0$
		$x_2 = \frac{4\epsilon_s^{*1/2}}{KT}(\epsilon^{1/2} + \epsilon_s^{*1/2})$
	Emission	$x_1 = 0$
		$x_2 = \frac{4\epsilon_s^{*1/2}}{KT}(\epsilon^{1/2} - \epsilon_s^{*1/2})$

In accord with the above approximation we have not distinguished between longitudinal and transverse phonons.

We have therefore assumed a squared matrix element given by

$$|H'|^2 = \frac{E_1^2 \hbar q}{2V\rho v_s}\begin{pmatrix} N_q \\ N_q + 1 \end{pmatrix}, \tag{A1}$$

where E_1 is the deformation-potential constant, V and ρ are the volume and the density of the crystal, v_s is the velocity of sound, and N_q is the phonon distribution; N_q or $N_q + 1$ must be taken for absorption or emission, respectively. By application of the golden rule, the matrix element in Eq. (A1) yields the scattering rate

$$P_{\text{ac}}\, d^3q = \frac{E_1^2 q}{8\pi^2 \rho v_s}\begin{pmatrix} N_q \\ N_q + 1 \end{pmatrix} \times \delta(\epsilon(\vec{k} \pm \vec{q}) - \epsilon(\vec{k}) \mp \hbar q v_s)\, d^3q\,, \tag{A2}$$

where the upper or lower sign must be taken for absorption or emission, respectively.

Transforming to the starred space [see Eq. (8)], we again make the spherical approximation

$$q = q^*\left(\frac{m_l}{m_0}\cos^2\theta^* + \frac{m_t}{m_0}\sin^2\theta^*\right)^{1/2} \approx q^*\left(\frac{m_D}{m_0}\right)^{1/2}, \tag{A3}$$

where θ^* is the angle between $\vec{q}^*$ and the principal axis of the valley, and m_D the density-of-state effective mass $(m_l m_t^2)^{1/3}$.

The argument of the δ of energy conservation then becomes

$$\frac{\hbar^2 q_*^2}{2m_0} \pm \frac{\hbar^2}{m_0} k^* q^* \cos\gamma \mp \hbar q^* (m_D/m_0)^{1/2} v_s\,, \tag{A4}$$

TABLE IV. Acoustic-scattering rates (see text); $\bar{x}$ has been used equal to 3.5 in the present calculations, according to Eq. (A7).

$\epsilon \leq \epsilon_s^*$	Absorption No emission	$P_{ac} = (A_a/\epsilon^{1/2})[\frac{1}{2}(x_2^2 - x_1^2) - \frac{1}{6}(x_2^3 - x_1^3) + \frac{1}{48}(x_2^4 - x_1^4) - \frac{1}{4320}(x_2^6 - x_1^6)]$
$\epsilon > \epsilon_s^*$	Absorption	$P_{ac} = \frac{A_a}{\epsilon^{1/2}}(\frac{1}{2}x_2^2 - \frac{1}{6}x_2^3 + \frac{1}{48}x_2^4 - \frac{1}{4320}x_2^6),\ x_2 < \bar{x}$
		$P_{ac} = \frac{A_a}{\epsilon^{1/2}}(\frac{1}{2}\bar{x}^2 - \frac{1}{6}\bar{x}^3 + \frac{1}{48}\bar{x}^4 - \frac{1}{4320}\bar{x}^6),\ x_2 \geq \bar{x}$
	Emission	$P_{ac} = \frac{A_a}{\epsilon^{1/2}}(\frac{1}{2}x_2^2 + \frac{1}{6}x_2^3 + \frac{1}{48}x_2^4 - \frac{1}{4320}x_2^6),\ x_2 < \bar{x}$
		$P_{ac} = \frac{A_a}{\epsilon^{1/2}}(\frac{1}{2}\bar{x}^2 - \frac{1}{6}\bar{x}^3 + \frac{1}{48}\bar{x}^4 - \frac{1}{4320}\bar{x}^6 + \frac{1}{3}x_2^3),\ x_2 \geq \bar{x}$

where γ is the angle between $\vec{q}^*$ and $\vec{k}^*$. As in the standard procedure,[7] the conditions of vanishing of this argument and of $|\cos\gamma| \leq 1$ yield the limits of variability of q^*. For our purposes it is more convenient to express these limits for the dimensionalless variable

$$x = \hbar q v_s / KT = (\hbar q^* v_s / KT)(m_D/m_0)^{1/2}. \tag{A5}$$

These limits are given in Table III where $\epsilon_s^* = \frac{1}{2}m_D v_s^2$. The transition rate is given by

$$P_{ac}\,dx = \frac{A_a}{\epsilon^{1/2}}\begin{pmatrix} N_q(x) \\ N_q(x)+1 \end{pmatrix} x^2\,dx, \tag{A6}$$

where

$$A_a = (E_1 m_D/4\hbar^2)(1/\pi\rho v_s) \times \left(\frac{KT}{\epsilon_s^{*\,1/2}}\right)^3. \tag{A6'}$$

At this point we must introduce an expression for $N_q(x)$. As mentioned above, this expression must be a very good approximation of the true N_q in order to have a correct description of the energy balance at low temperatures. We found that a suitable approximation is given by the following truncated Laurent expansion:

$$N_q(x) \approx \begin{cases} 1/x - \frac{1}{2} + \frac{1}{12}x - \frac{1}{720}x^3, & x < 3.5 \\ 0, & x \geq 3.5. \end{cases} \tag{A7}$$

The integration of the scattering rate in Eq. (A6) can then be performed very easily, and the resulting scattering rates are given in Table IV.

For the determination of the state after scattering, the expression of $P_{ac}\,dx$ in Eqs. (A6) and (A7) has been used to choose x with the aid of the rejection technique.[6] Once x has been determined, q^* is obtained by Eq. (A5), and then the direction of the transformed electron wave vector $\vec{k}'^*$ after scattering is obtained by simple geometrical considerations of energy and momentum conservation. The angle of rotation around the direction of $\vec{k}^*$ has been taken as completely random, according to Eq. (A2).

Intervalley scattering

The scattering mechanism is treated here in the traditional way.[6,40] The total scattering rate is given by

$$P_{iv} = \begin{cases} A_{iv} N_i (\epsilon + \hbar\omega_i)^{1/2} & \text{(absorption)} \\ A_{iv}(N_i + 1)(\epsilon - \hbar\omega_i)^{1/2} & \text{(emission)} \end{cases}, \tag{A8}$$

where

$$A_{iv} = D_i^2 m_D^{3/2} z_i / \sqrt{2}\,\pi\rho\hbar^3\omega_i; \tag{A8'}$$

D_i and $\hbar\omega_i$ are the coupling constant and the phonon energy (assumed constant) of the considered ith mechanism; Z_i is the number of possible final valleys ($Z_i = 4$ for f scattering; $Z_i = 1$ for g scattering). The final valley in case of f scattering is chosen randomly among the four possible ones, while in case of g scattering it is unequivocally determined by the initial valley; the states after scattering are taken as equally probable on the shell of energy conservation.

Ionized impurity scattering

By assuming a screened Coulomb potential due to charge $\pm e$,

$$V(r) = \pm (e^2/\kappa r) e^{-\beta r}, \tag{A9}$$

where r is the distance from the impurity center, κ the dielectric constant, and β the inverse screening length, the scattering probability per unit time a state $\vec{k}$ to a state in $d\vec{k}'$ is given, by the golden rule, by[55]

$$P_I(\vec{k}\vec{k}')\,d^3k' = (4e^2 N_I/\kappa^2\hbar) \times \{\delta(\epsilon' - \epsilon)/[\beta^2 + (\vec{k}' - \vec{k})^2]^2\}, \tag{A10}$$

where N_I is the impurity concentration.

With the Hearring and Vogt transformation and the approximation in Eq. (A3), we obtain

$$P_I(k^*, \cos\gamma)d(\cos\gamma) = \frac{8\sqrt{2}\,\pi m_D^{3/2} e^4 N_I}{\kappa^2 \hbar^4 \beta^4} \times \frac{\epsilon^{1/2}}{\left[1 + \frac{4m_D}{\hbar^2\beta^2}\epsilon(1-\cos\gamma)\right]^2}, \tag{A11}$$

which yields a total scattering rate

$$P_I = A_I \frac{\epsilon^{1/2}}{1 + \frac{8m_D\epsilon}{\hbar^2\beta^2}}, \tag{A12}$$

where

$$A_I = \frac{16\sqrt{2}\,\pi m_D^{3/2} e^4 N_I}{\kappa^2 \hbar^4 \beta^4}. \tag{A12'}$$

Equation (A11) can be used to generate scattering angles γ with the direct technique.[41] With a random number r between 0 and 1 we generate the scattering angle γ_r given by

$$\cos\gamma_r = 1 - \frac{2(1-r)}{1 + \frac{8m_D\epsilon r}{\hbar^2\beta^2}}. \tag{A13}$$

The screening length β^{-1} has been assumed equal to half the average distance d between impurities. In fact, due to compensation, at low temperatures, in the materials considered here, there are no electrons to screen the ions, but, according to the Conwell and Weisskopf[7] idea, only the impurity center closest to the electron is taken into account. This is substantially equivalent to say that the impurity is screened at a distance equal to half d.

*Partially supported by Consiglio Nazionale delle Ricerche, Italy.

[1]C. B. Norris and J. F. Gibbons, IEEE Trans. Electron Devices ED-14, 38 (1967).
[2]W. E. Spear, J. Non-Cryst. Solids 1, 197 (1969).
[3]A. Alberigi Quaranta, C. Jacoboni, and G. Ottaviani, Riv. Nuovo Cimento 1, 445 (1971).
[4]M. Martini, J. W. Mayer and K. R. Zanio, in *Applied Solid State Science*, edited by Wolfe (Adademic, New York, 1972), Vol. 3.
[5]C. Canali, G. Ottaviani, and A. Alberigi Quaranta, J. Phys. Chem. Solids 32, 1707 (1971).
[6]W. Fawcett, A. D. Boardman, and S. Swain, J. Phys. Chem. Solids 31, 1963 (1970).
[7]E. M. Conwell, in *Solid State Physics*, edited by F. Seitz and D. Turnbull (Academic, New York, 1967), Suppl. 9.
[8]M. Asche and O. G. Sarbei, Phys. Status Solidi 33, 9 (1969).
[9]T. Braggins (private communication).
[10]The measurements were performed by the Laboratoire d'Analyse par Reactions Nucleaires, C.E.N., Saclay, France.
[11]A. Alberigi Quaranta, C. Canali, and G. Ottaviani, Rev. Sci. Instrum. 41, 1205 (1970).
[12]C. Canali, G. Ottaviani, A. Taroni, and G. Zanarini, Solid State Electron. 14, 661 (1971).
[13]H. Lemke and G. O. Muller, Phys. Status Solidi 24, 127 (1967).
[14]P. Norton, T. Braggins, and H. Levinstein, Phys. Rev. B 8, 5632 (1973).
[15]E. H. Putley and W. H. Mitchell, Proc. Phys. Soc. Lond. A 72, 193 (1958).
[16]D. Long and J. Myers, Phys. Rev. 115, 1107 (1959).
[17]R. A. Logan and A. J. Peters, J. Appl. Phys. 31, 122 (1960).
[18]D. Long, Phys. Rev. 120, 2024 (1960).
[19]C. Jacoboni, C. Canali, G. Ottaviani, and A. Alberigi Quaranta, *Proceedings of the 12th International Conference on the Physics of Semiconductors*, edited by M. H. Pilkuhn (Teubner, Stuttgart, 1974).
[20]M. Asche and O. G. Sarbei, Phys. Status Solidi A 8, K61 (1971).
[21]M. H. Jørgensen, N. O. Gram, and N. I. Meyer, Solid State Commun. 10, 337 (1972).
[22]M. Asche and O. G. Sarbei, Phys. Status Solidi B 46, K121 (1971).
[23]N. O. Gram, Phys. Lett. A 38, 235 (1972).
[24]V. Rodriguez and M. A. Nicolet, J. Appl. Phys. 40, 496 (1969).
[25]C. Canali and G. Ottaviani, Phys. Lett. A 32, 147 (1970).
[26]M. Costato and L. Reggiani, J. Phys. C 5, 159 (1972).
[27]C. Herring and E. Vogt, Phys. Rev. 101, 944 (1956).
[28]H. W. Streitwolf, Phys. Status Solidi 37, K47 (1970).
[29]M. Lax and J. L. Birman, Phys. Status Solidi B 49, K153 (1972).
[30]J. R. Haynes, M. Lax, and W. F. Flood, J. Phys. Chem. Solids 8, 392 (1952).
[31]W. P. Dumke, Phys. Rev. 118, 938 (1960).
[32]N. O. Folland, Phys. Rev. B 1, 1648 (1970).
[33]A. Onton, Phys. Rev. Lett. 22, 288 (1969).
[34]J. C. Portal, L. Eaves, S. Askenazy, and R. A. Stradling, Solid State Commun. 14, 1241 (1974); and *Proceedings of the 12th International Conference on the Physics of Semiconductors*, edited by M. H. Pilkuhn (Teubner, Stuttgart, 1974).
[35]P. J. Price and R. L. Hartmann, J. Phys. Chem. Solids 25, 567 (1964).
[36]L. Bacchelli-Montefusco and C. Jacoboni, Solid State Commun. 10, 71 (1972).
[37]I. Jäger, Phys. Status Solidi B 61, 711 (1974).
[38]M. Asche, B. L. Boichenko, V. M. Bondar, and O. G. Sarbei, Phys. Status Solidi B 44, 173 (1971).
[39]J. G. Nash and J. W. Holm-Kennedy, Appl. Phys. Lett. 24, 139 (1974).
[40]W. Fawcett and E. C. S. Paige, J. Phys. C 4, 1801 (1971).
[41]V. Borsari and C. Jacoboni, Phys. Status Solidi B 54.

649 (1972).
[42]C. Hammar, Phys. Rev. B 4, 417 (1971).
[43]W. Fawcett and H. D. Rees, Phys. Lett. A 29, 578 (1969).
[44]A. Alberigi-Quaranta, V. Borsari, C. Jacoboni, and G. Zanarini, Appl. Phys. Lett. 22, 103 (1973).
[45]B. N. Brockhouse, Phys. Rev. Lett. 2, 256 (1959). The equivalent temperatures of intervalley phonons are determined by the location of the valley minima and by the dispersion curve of the considered branch; see Ref. 18.
[46]J. C. Hensel, H. Hasegawa, and N. Nakayama, Phys. Rev. 138, A225 (1965).
[47]M. Costato and L. Reggiani, Phys. Status Solidi 42, 591 (1970).
[48]J. J. Hall, Phys. Rev. 161, 756 (1967).
[49]W. C. Dunlap and R. L. Watters, Phys. Rev. 92, 1396 (1953).
[50]We do not consider mode-I and mode-II phonons; in the present model their introduction would simply add new intervalley phonons with slightly different equivalent temperatures.
[51]In a detailed discussion of their results, Norton *et al.* (Ref. 14) have actually found that the introduction of low-energy intervalley phonons improves also the agreement between theory and their Ohmic mobility results.
[52]D. Schweitzer and K. Seeger, Z. Phys. 183, 207 (1965).
[53]J. W. Holm-Kennedy and K. S. Champlin, Appl. Phys. Lett. 16, 46 (1970).
[54]L. E. Vorobyov, V. I. Stafeev, and A. U. Ushakov, Phys. Tech. Semicond. 7, 919 (1973).
[55]J. G. Ruch and W. Fawcett, J. Appl. Phys. 41, 3843 (1970).